ISSN: 0974-5823 Vol. 7 No. 1 January, 2022

International Journal of Mechanical Engineering

Mechanical Properties of Wire Arc Additive Manufacturing ER4043-AlN composites

P. Kumar
Department of Mechanical Engineering, Jawaharlal Nehru Technological University Anantapur, Ananthapuramu 515002, Andhra Pradesh, India

A. Mahamani
Department of Mechanical Engineering, Sri Venkateswara College of Engineering and Technology, R V S Nagar, 517127, Andhra Pradesh, India

B. Durga Prasad
Department of Mechanical Engineering, Jawaharlal Nehru Technological University Anantapur, Ananthapuramu 515002, Andhra Pradesh, India

Abstract

Wire + arc additive manufacturing (WAAM) was used to build the AA6061-AlN components formed by feeding wires and adding AlN powder. Preparation of the specimen in longitudinal and transvers direction with 0%, 2.5%, 5%, and 7.5% ratios. This paper evaluates the reinforcing weight %, tensile, EBSD, and fracture surface analysis results. This study investigates the influence of orientation, the microstructure, mechanical characteristics, and hardness of the bar in both the longitudinal and transverse orientations. Fe-rich interlayer phases were more closely linked to fracture initiation in the heat-treated condition for both orientations and composite materials. It was discovered that additive made bar had a greater transverse yield strength, ultimate strength, and hardness.

Keywords: Additive Manufacturing, Tensile, EBSD, Grain Size, Fracture Surface

Introduction

Wire-arc additive manufacturing (WAAM) is a technology for creating metal components that deposits elements directly and locally on metal components, layer by layer [1]. In recent years, Wire + Arc Additive Manufacturing (W+AAM) has shown its potential to build fully-dense large-scale metal objects at an affordable price by employing high-quality wire as a feedstock [2]. Compared to conventional manufacturing technologies, WAAM can effectively create components with complicated geometry. [3]. Because of its cheap cost and high disposal rate, wire arc additive manufacturing (WAAM) is viable. [4]. It is possible to build huge components at high rates (many kilogrammes per hour) using wire arc ALM, a new technique. [5]. We have developed a new metal component additive manufacturing technology called Wire Arc Additive Manufacturing. [6]. However, both wire-based and powder-based methods require nearly the same amount of energy. Consequently, Deposition energy requirement in wire-based processes is 85 percent, whereas powder-based processes need 70 percent of the energy needed for deposition in powder-based processes [7]. The thermal conductivity of AlN is particularly high, despite the fact that it has many of the same characteristics as other metals. In addition, the near lattice match between AlN & Al ensures its high adhesion, making it worthwhile to study its load-bearing potential. When making composites, powder metallurgy or melt metallurgy are used [8, 9]. Properly distributed nanostructured AlN particles improve mechanical characteristics [10]. The mechanical qualities of the joint constructed using the ER4043 improved. Compared to the junction created with ER5356, the Al A6061 with ER4043 welded common has an advantage because of the excellent grain conformation and somewhat scattered porosity in the weld region [11]. The fusion zone (FZ) of an ER4043 welded sample has a lower grain size than that of an ER5356 welded sample, according to microstructure study [12]. Component qualities were studied to determine how much deposition rate could be raised without producing any failures or defects [13]. Anisotropy was shown to be evident in both the perpendicular and parallel deposition directions

in terms of the material's strength, elongation, & ultimate tensile strength [14]. In the vertical direction, the qualities were a little lower. The tensile characteristics of the deposit were found to be anisotropic [15]. There is interest and demand for WAAM technology to produce high strength aluminium alloy from several industries. Different factors of aluminium alloys are being researched in WAAM technology, such as heat sources, wires, process parameters, & post-treatments, which aim to impact the formation, microstructure, and mechanical properties of the components.

Experimental procedure

The structure's filler material was ER4043 aluminium alloy wire with a diameter of 1.2 millimeters, which was employed as a substrate for the aluminium alloy 6061. Table 1 displays the substrate and wire compositions. Aluminium nitride Composites (AlNCs) were made using WAAM using Metal Inert Gas (MIG) welding-based forms of welding, both without and with AlN powder between layers. AlN particles were blended with 100% ethanol before being coated with an identical weight percentage between layers. The wire feeding speed was set at 4.8 m/min, and both the travel speed (500 mm/min) to the flow rate of 99.99% argon shielding gas (15 L/min) was kept constant. AlNCs had 7 layers and measured 200 mm 150 mm 15mm. The WAAM experimental setup are shown in Figure 1. Test specimen samples are shown in the Figure 2. The WAAM fabricated composite samples are allowed in heat treatment process kept with 700^0C with a time interval of 2 hours in each specimen. Then, the heat treated specimen surface was machined using the vertical turret milling machine. However, those machined surfaces are cut in to required specific sizes, then characterized by SEM (model: JEOL 6360 LV) and EBSD were analyzed.

Table 1. Machine parameter (MP)

Welder type	MIG (Metal Inert Gas)
Electrode	Metal–rare earth, ER4043, 1.2 mm diameter
Substrate plate	AA6061
Substrate plate dimensions	200 x 150 x 15mm
Welding current	150A
Distance between electrodes and base plate	25 mm
Aluminum-silicon alloy filler wire grade (feedstock)	ASTM Grade 1
Wire diameter	1.2 mm
Wire feed rate	1.5 m/min
Deposition rate	150 mm/min
Number of layers	7
Average layer height	8mm
Cooling time for the layer to layer	45 minutes
Shielding gas	Shielding gas

Figure 1 Experimental set up

Figure 2 Sample specimens

Characterization of AA6061-AlN**composites**

Microstructure and energy dispersive analysis

Figure 3(a,c,e,g) shows the electron micrograph and spectral energy dispersion measurements of the AA6061-AlN composites cut in the direction of flow of the wire arc, i.e. X direction. Figure 3(a,c,e,g) shows SEM (scanning electron micrographs) of 0.0 %, 02.5 %, 0.5 %, & 07.5 % composites in the X-direction, respectively. The micrographs reveal a uniform distribution of AlN particles with no apparent clustering. There is no question about the link between the reinforcements and the matrix in this design.
Figure 3 (b, d, f, h) shows the specimen sliced perpendicular to the low of the wire arc, i.e. in the Y direction. Figures 3(b, d, f, h) show scanning electron micrographs of 0.0 %, 02.5 %, 0.5 %, & 07.5 % composites in the Y direction. The micrographs show that the AlN particles be cluster-free too equally distributed throughout the matrix. As a result, the matrix-reinforcement interactions are clear, and the reinforcements are pure.

X-0%

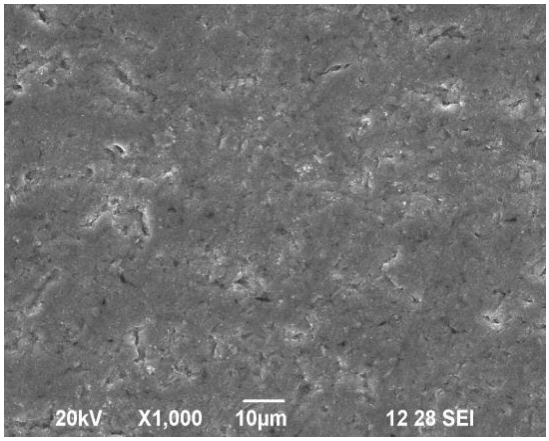

Figure 3 (a)

Y-0%

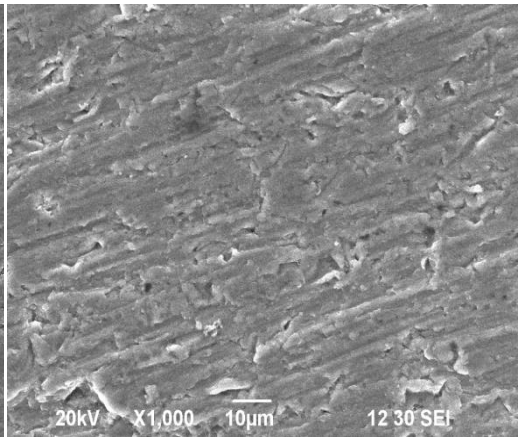

Figure 3 (b)

X-2.5% **Y-2.5%**

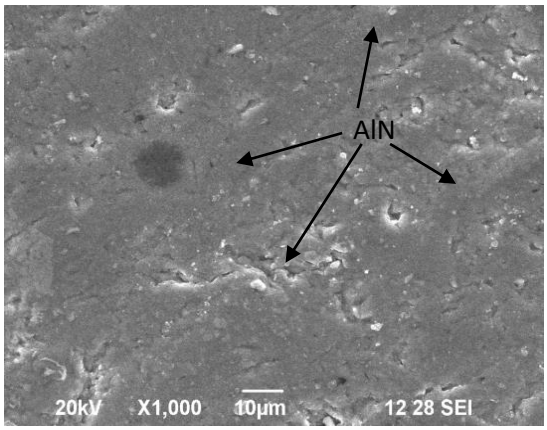

Figure 3 (c)

X-5%

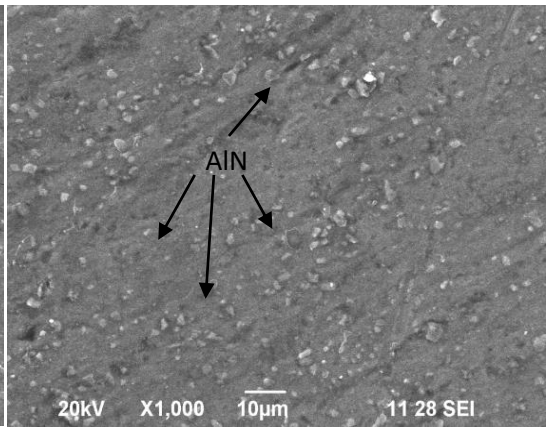

Figure 3 (d)

Y-5%

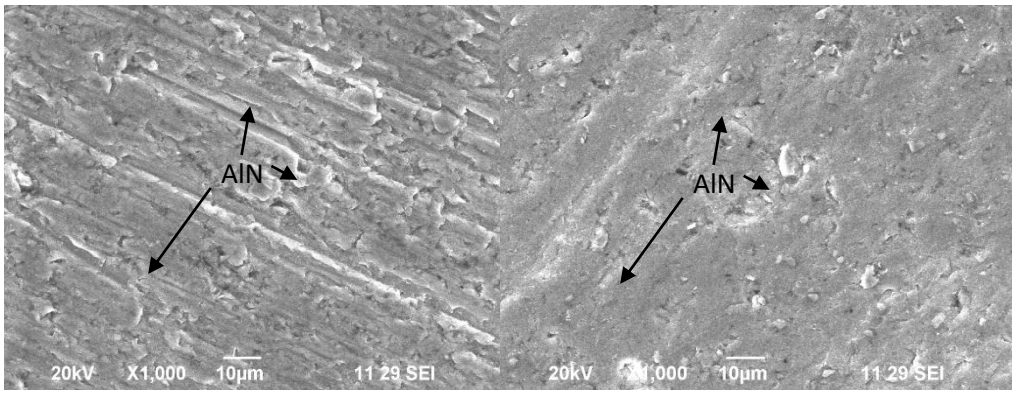

Figure 3 (e)

X-7.5%

Figure 3 (f)

Y-7.5%

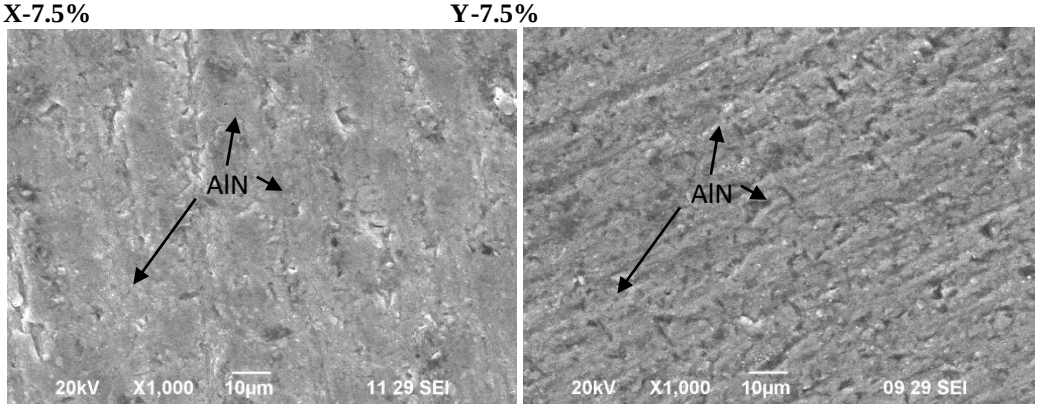

Figure 3 (g)

Figure 3 (h)

EBSD analysis of AA6061-AlN**composites**

Electron Back Scattering Diffraction (EBSD) is an SEM function that is commonly used to investigate grain orientation and crystal structure of various materials. [16] Provides a concise overview of EBSD. Figures 4(a, e, i) epitomize that the EBSD of 2.5%, 5% and 7.5% composites in X-direction, respectively. Figures 4(c, g, k) is the specimen cuts perpendicular to the low of wire arc i.e Y direction. Figures 4(b, d, f) epitomize that the EBSD micrographs of 2.5%, 5% and 7.5% composites in X-direction, respectively. Figures 4(h, j, l) are the specimen cuts perpendicular to the low of wire arc i.e Y direction. Figures 4(a,c, e,g,i,k) & 4(b,d,f,h,j,l) show EBSD images of ER 4043 and AlN composites created using the Wire Arc Additive Manufacturing Process. EBSD photos vividly show the material's existing coarse structure.

Fig. 1 shows EBSD pictures of the as-received ER4043 aluminium alloy and AlN particles. The nature of grain structure before and after aluminium and AlN fraction particles is depicted in this image. Pure aluminium has a coarse grain structure with numerous twins. Grains had an average diameter of 13.66 microns, with an area fraction of around 0.011. The composite has an average grain size of 2.8

microns & features a tiny granular structure. The composite's grain size was significantly decreased. Two aspects of plastic deformation, one related to stirring rate, and one related to AlN particles' ability to cause pinning action, all affect grain size during FSP.

Figure 1 shows EBSD maps of ER4043 aluminium alloy and AlN particles. The maps show the grain structure too the influence of AlN particle weight %. The black spots in Fig. show where AlN particles are located. Grain structure was altered as a consequence of the synthesis of AlN. With a rise in the percentage of AlN particles in a sample, grains get smaller. Figure 1 shows this clearly. The average grain size of the composite was 165 m & 78 m, respectively, for 0 percent AlN particles, 2.5 percent AlN particles, 5 percent AlN particles, and 7.5 percent AlN particles. The following describes the phenomena of grain refining. When AlN particles are added to a composite melt, their formation changes the solidification process. They serve as nucleation points for grains in the aluminium melt because they are suspended. The unrestricted growth of -aluminium grains is hindered by the presence of AlN particles. In the composite, their expansion is limited, and the grain size is minimised.

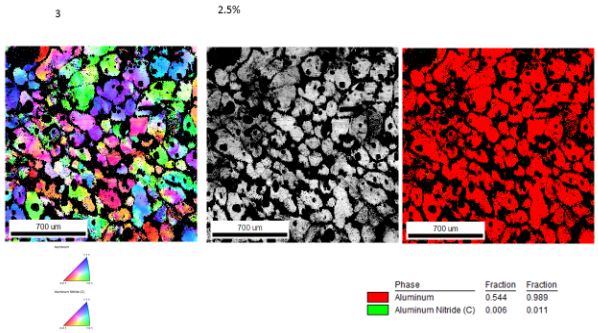

Figure 4 (a)

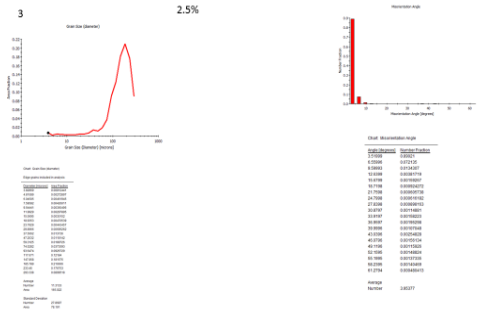

Figure 4 (b)

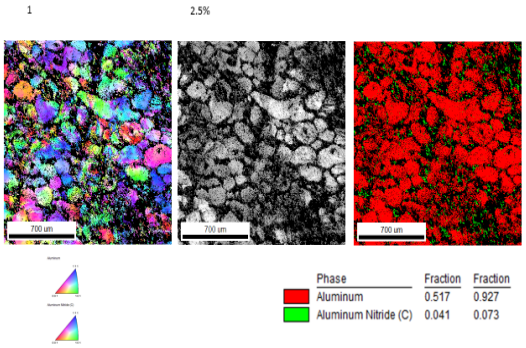

Figure 4 (c)

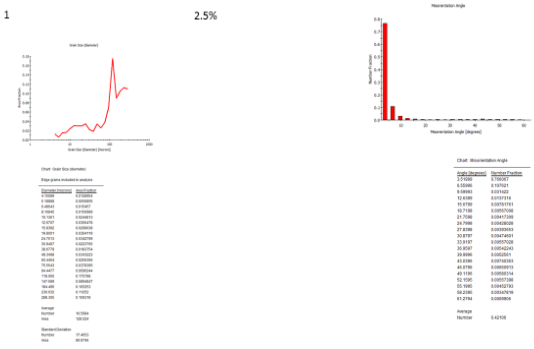

Figure 4 (d)

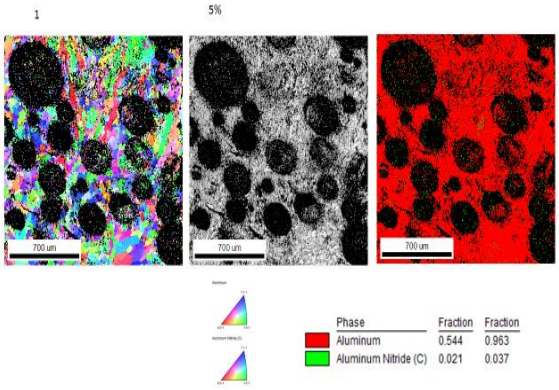

Figure 4 (e)

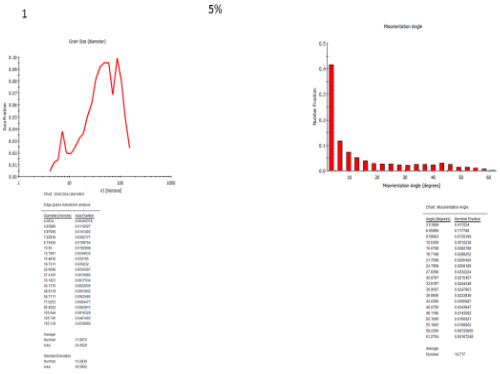

Figure 4 (f)

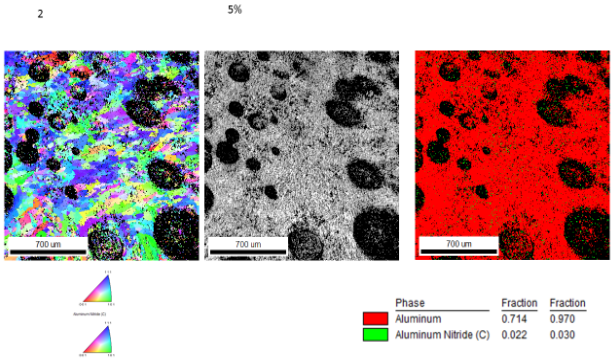

Figure 4 (g)

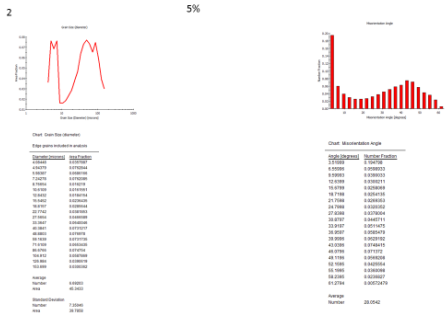

Figure 4 (h)

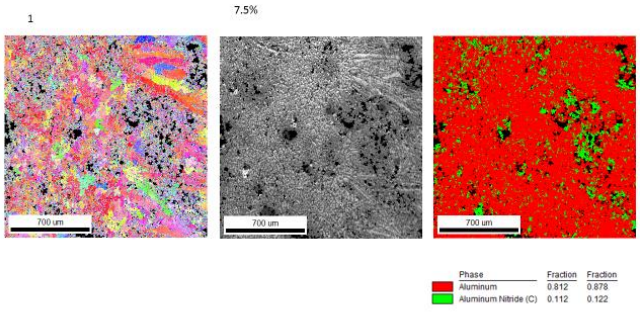

Figure 4 (i)

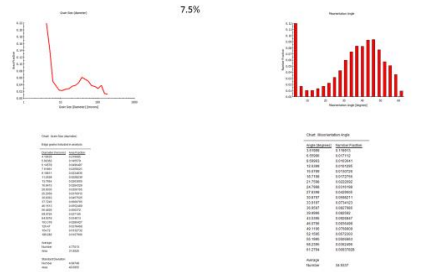

Figure 4 (j)

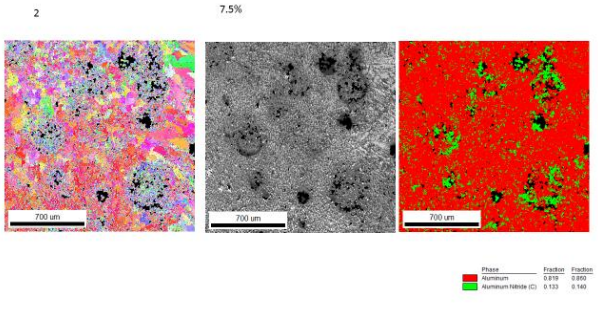

Figure 4 (k)

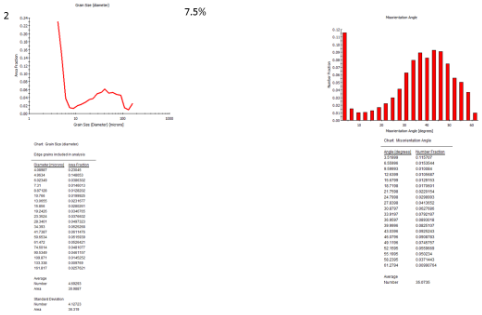

Figure 4 (l)

Grain size

The grain size of the AA6061-AlN composites at various reinforcement ratios was evaluated in Table 2. The AA6061-AlN composite has a lower grain size than the AA6061 alloy at other reinforcement ratios in both cutting directions (X & Y) Figure 5. Shows that the reinforcement increases there is the decrease in grain size regardless of the wt % of the reinforcement, increasing the reinforcement ratio induces a significant drop in the average grain size of composites. In both cases, transverse direction grains were polished more than longitudinal direction grains [17].

Table 2 Average grain size

Grain Size(µm)	0	2.5	5	7.5
X (cut the specimen perpendicular to the flow of wire travel)	41.26	34.43	24.07	17.61
Y (cut the specimen in the direction of flow of wire travel)	45.46	36.68	28.92	19.09

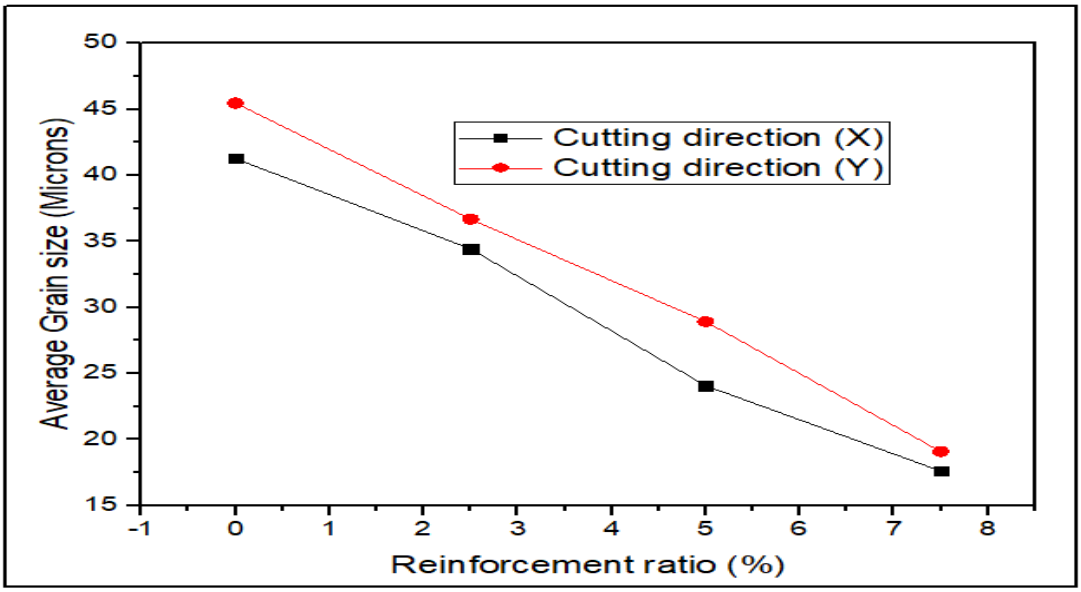

Figure. 5 Grain Size

Influence of Tensile strength

The tensile strength of various AA6061-AlN composites was tabulated in Table 3 and tensile tested specimens are shown in Figure 6. As can be seen in Figure 7, increasing the reinforcement causes a rise in the tensile strength of all reinforced materials. However, the tensile strength of AA6061-AlN composite contracts expressively compared with the AA6061 pure alloy. The production of fine grains, which improves the material's hardness. Furthermore, when the composite is pushed over the counter surface, the presence of AlN particles causes the flow of matrix material to be restricted. That crack deflection is related to grain direction. It has been discovered that fracture propagation is connected to grain disorientation. [18] As we all know, fracture propagation seeks the path needing the least amount of energy; hence, AlN with finer and disordered grains is beneficial to tensile characteristics.

Anisotropic strength geste is seen at room temperature in the primarily textured structure caused by guided grain production. The mechanical characteristics in the plastic distortion region are determined by the Build Direction (BD), which cannot be described just by grain structure. As shown in Figure. 8, different mechanical characteristics are obtained in various directions concerning the BD in the as-welded state. With a sample size of 3 5 samples, it is obvious that in the test direction 45° to BD (Y-X), there is a rise in both the tensile and yield strength as well as an overall decrease in the extension of the material. The material has a decreased strength and greater plastic deformability in the deposit direction (Y) and the BD direction (X). The shift in test direction of 45 ° (Y-X) leads in an increase in tensile strength of around 96 – 123 MPa. The yield strength increases by around 109 MPa, whereas the fracture strain decreases by approximately 1 – 4. Due to the wide range of observed values, in order to make sense of this data, one must look at it as an overall trend. High-temperature anisotropy items are not available; anisotropy causes in the current material's room temperature range are based on crystallographic anisotropy. Elastic and plastic deformation literature is replete with studies using cubic crystals. Both the elasticity modulus (19, 20) and the temperature-dependent confirmation of the strength characteristics (21, 22) are instances of directional dependency.

Figure 6 Tensile tested specimens

Table 3 TS (Tensile strength)

Ultimate Tensile Strength (N/mm^2 or Mpa)	0	2.5	5	7.5
X (cut the specimen perpendicular to the flow of wire travel)	95	103	108	122
Y (cut the specimen in the direction of flow of wire travel)	97	104	109	124

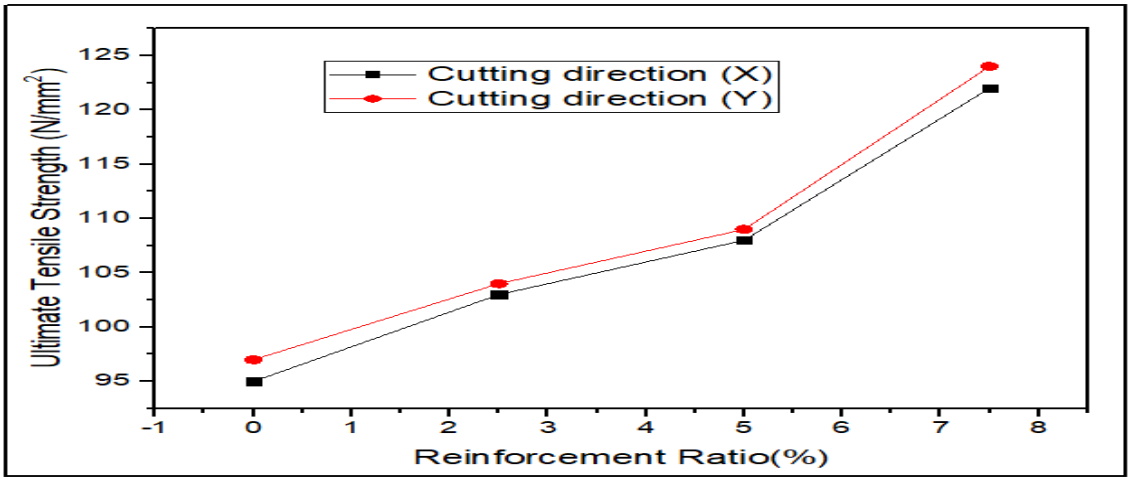

Figure.7 TS

Influence of Yield strength

The yield strength of the AA6061-AlN composites at various reinforcement ratio was evaluated in Table 4 & Figure 8. Shows that the yield strength of AA6061-AlN composite is higher than that of the AA6061 alloy at other reinforcement ratios in both cutting directions (X & Y). Regardless of the wt % of the reinforcement, the inverse of the longitudinal Compared to the longitudinal axis, the granules were finer; increasing the reinforcement ratio generates a significant rise in the yield strength of composites. As a result of this variation in microstructure, the yield and tensile strength of transverse samples were greater than longitudinal samples [23]. As a result, these particles readily separate from the matrix, reducing the material's stiffness. As a result, the yield strength of composites increases. Figure 8 shows that the interfacial strength of AlN with the AA6061 matrix is greater, limiting the yield strength.

Table 4 yield strength

Yield strength	0	2.5	5	7.5
X (cut the specimen perpendicular to the flow of wire travel)	45	53	68	76
Y (cut the specimen in the direction of flow of wire travel)	47	56	72	81

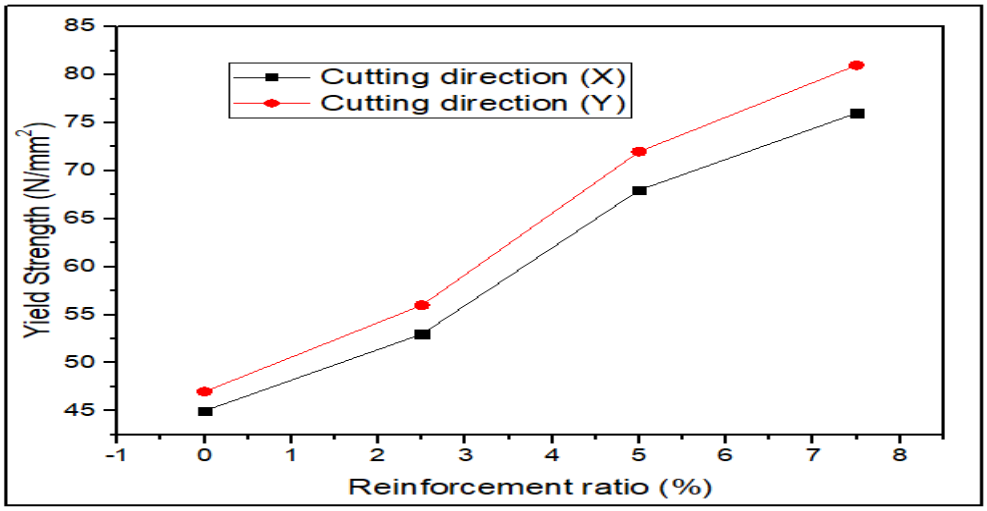

Figure.8 yield strength

Percentage of elongation

The percentage elongation of the AA6061-AlN composites at various reinforcement ratio was evaluated in Table 5. Figure 9 shows that the percentage elongation of AA6061-AlN composite is lower than that of the AA6061 alloy at other reinforcement ratios in both cutting directions (X & Y). The percentage elongation of composite materials decreases significantly as the reinforcement ratio is increased, regardless of the weight percent of the reinforcing. Samples met the criteria in the horizontal stress direction; however the vertical stress direction elongation was lower than predicted. A reason that merits further examination is the presence of porosity and an irregular microstructure in the fusion zone of single layers.

Table 5 Percentage of elongation

Percentage of elongation	0	2.5	5	7.5
X (cut the specimen perpendicular to the flow of wire travel)	7.21	6.78	5.87	4.28
Y (cut the specimen in the direction of flow of wire travel)	6.92	6.35	5.24	4.07

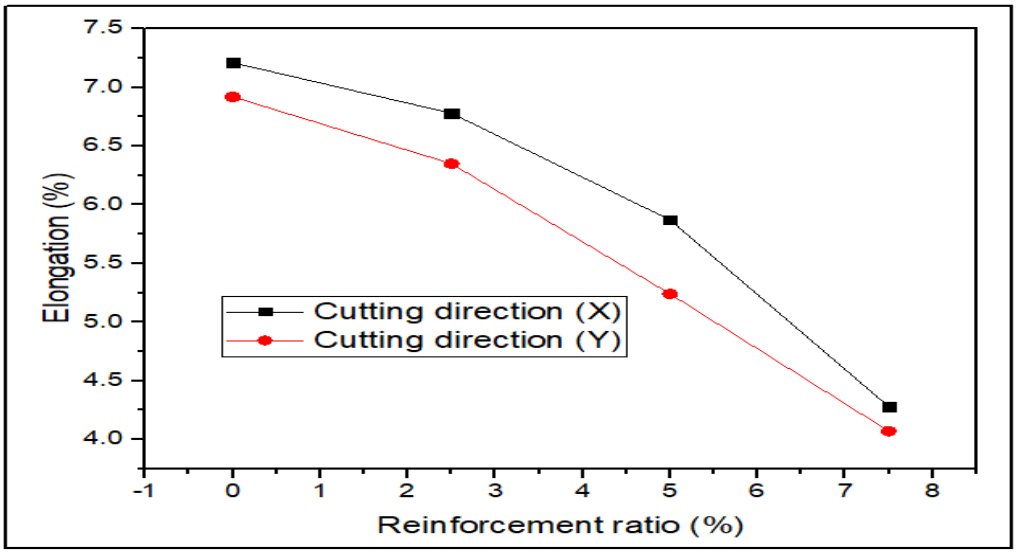

Figure: 9 Percentage of elongation

Fracture surface analysis

The fracture surface analysis of the AA6061-AlN composites at various reinforcement ratios for tensile specimens in the X direction as shown in Figure 10 (a, c, e, g). Figure 10 (b, d, f, g) shows the fractured SEM image for the cutting direction Y. Representative electron micrographs of the fracture surfaces clearly show the fractured surface area due to the variation in average grain size for both directions well as for composite materials. Fracture surfaces were identical in horizontal and vertical directions, with no discernible deviations. Furthermore, failure was uniformly dispersed throughout the buildup direction, with no discernible pattern, emphasising homogenous material qualities. The fracture surface was characterised predominantly by pits, indicating a ductile fracture. Micro pores were also embedded in the fracture surface morphology [24].

0% X **0%Y**

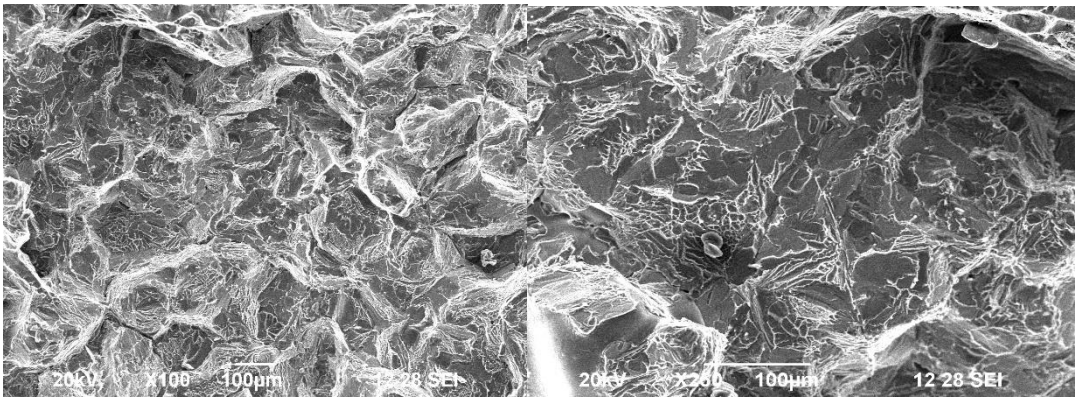

Figure 10 (a) Figure 10 (b)

2.5% X **2.5% Y**

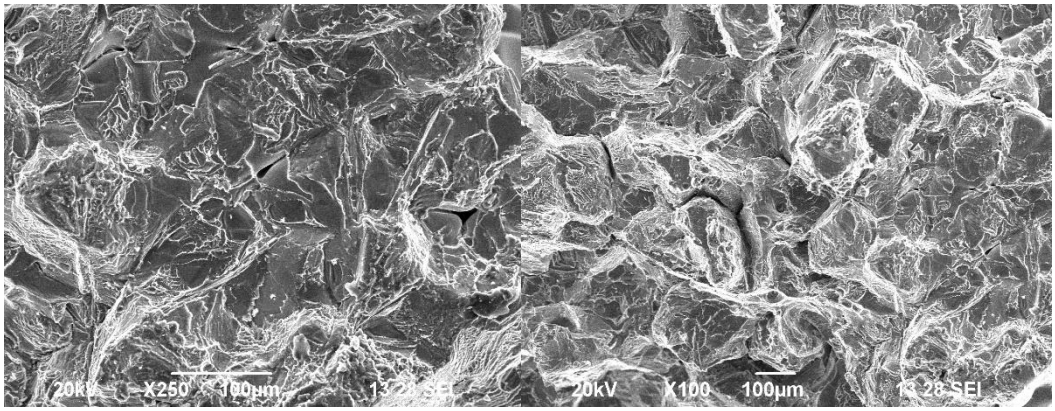

Figure 10 (c) Figure 10 (d)

5% X **5% Y**

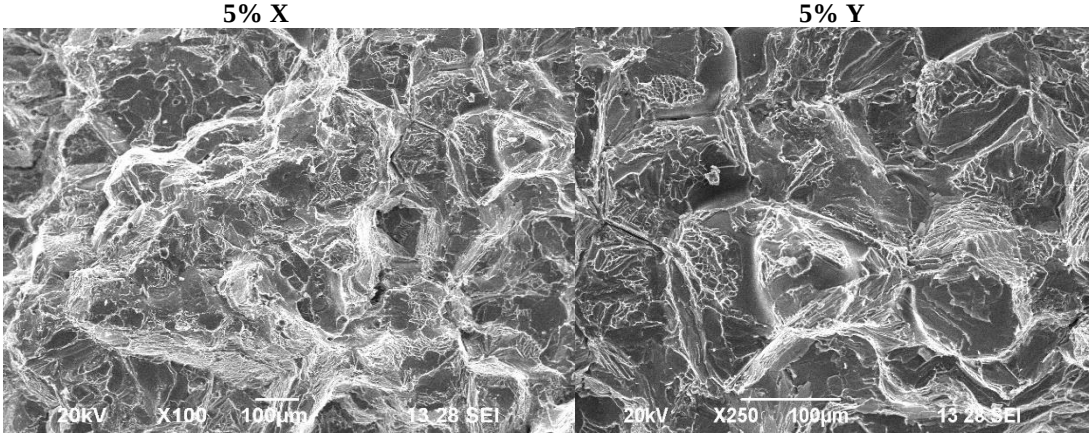

Figure 10 (e) Figure 10 (f)

7.5% X **7.5% Y**

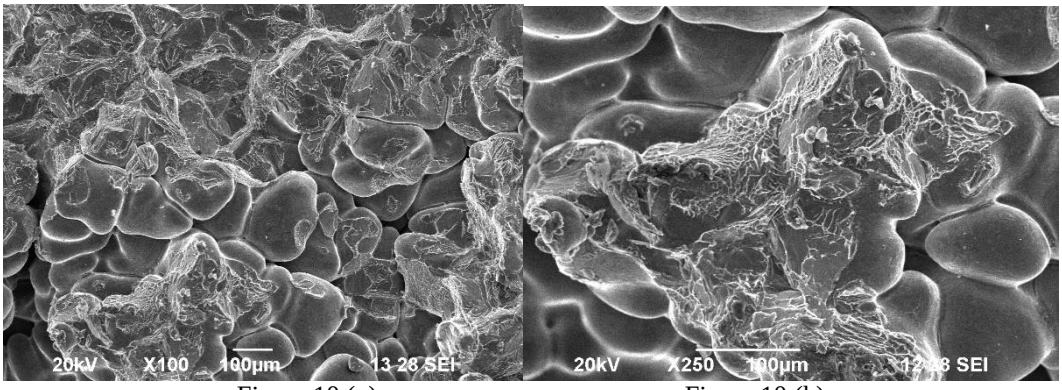

Figure 10 (g) Figure 10 (h)

Conclusions

The current study on AA6061-AlNcomposites, their characterization, and mechanical characteristics has yielded key findings: • Scanning Electronic Microscopy, EBSD, and Fracture surface investigations validated the presence and distribution of AlN reinforcements.

- When the temperature between passes is maintained constant, the material properties are evenly spread across the buildup geometry.
- Coordination system modifications are required for crystal growth directions so that elongation and strength reserves may be used.
- Cracks developed along extensive netlike second phases following initiation during tensile testing. Furthermore, netlike second phases lacked directionality. As a consequence, the as-deposited wall construction had no mechanical property anisotropy.

- It was more difficult to deform Fe-rich phases than alpha-Al, which was more malleable. There were more cracks in interlayer locations with Fe-rich phases after the material had been heat-treated. Furthermore, the tensile loading force was perpendicular to interlayer areas along the construction direction.
- Mechanical characteristics were decreased in the direction of deposition. As a consequence, the heat-treated wall structure exhibited mechanical property anisotropy.
- Grain size should be decreased whereas the reinforcement ratio increases as the tensile and yield strength increase.
- EBSD results confirm the presence of reinforcement and homogeneity.
- The percentage of elongation decreased as increased in reinforcement and fracture surface analysis shows up the course groove and fine groove of fractured specimens

REFERENCES:

[1] N. Chelah and M. H. Hussin, "Influence of Alloying Element in Filler Metal on Mechanical Properties of A6061 Al Alloy Welded Joints," *Int. J. Eng. Adv. Technol.*, vol. 9, no. 3, pp. 661–666, 2020, doi: 10.35940/ijeat.b2818.029320.

[2] M. N. M. Salleh, M. Ishak, L. H. Shah, and S. R. A. Idris, "The effect of ER4043 and ER5356 filler metal on welded Al 7075 by metal inert gas welding," *High Perform. Optim. Des. Struct. Mater. II*, vol. 1, no. Hpsm, pp. 213–224, 2016, doi: 10.2495/hpsm160191.

[3] F. Martina, J. Ding, S. Williams, A. Caballero, G. Pardal, and L. Quintino, "Tandem metal inert gas process for high productivity wire arc additive manufacturing in stainless steel," *Addit. Manuf.*, vol. 25, no. January, pp. 545–550, 2019, doi: 10.1016/j.addma.2018.11.022.

[4] Z. Qi, B. Qi, B. Cong, and R. Zhang, "Microstructure and mechanical properties of wire + arc additively manufactured Al-Mg-Si aluminum alloy," *Mater. Lett.*, vol. 233, pp. 348–350, 2018, doi: 10.1016/j.matlet.2018.09.048.

[5] N. Brodusch, H. Demers, M. Trudeau, and R. Gauvin, "Acquisition parameters optimization of a transmission electron forward scatter diffraction system in a cold-field emission scanning electron microscope for nanomaterials characterization," *Scanning*, vol. 35, no. 6, pp. 375–386, 2013, doi: 10.1002/sca.21078.

[6] Y. Q. Chen, S. P. Pan, M. Z. Zhou, D. Q. Yi, D. Z. Xu, and Y. F. Xu, "Effects of inclusions, grain boundaries and grain orientations on the fatigue crack initiation and propagation behavior of 2524-T3 Al alloy," *Mater. Sci. Eng. A*, vol. 580, pp. 150–158, 2013, doi: 10.1016/j.msea.2013.05.053.

[7] R. N. Ghosh, R. V. Curtis, and M. McLean, "Creep deformation of single crystal superalloys-modelling the crystallographic anisotropy," *Acta Metall. Mater.*, vol. 38, no. 10, pp. 1977–1992, 1990, doi: 10.1016/0956-7151(90)90309-5.

[8] P. Haasen, "Plastic deformation of nickel single crystals at low temperatures," *Philos. Mag.*, vol. 3, no. 28, pp. 384–418, 1958, doi: 10.1080/14786435808236826.

[9] M. Shunmugavel, A. Polishetty, and G. Littlefair, "Microstructure and Mechanical Properties of Wrought and Additive Manufactured Ti-6Al-4V Cylindrical Bars," *Procedia Technol.*, vol. 20, no. July, pp. 231–236, 2015, doi: 10.1016/j.protcy.2015.07.037.

[10] M. Köhler, S. Fiebig, J. Hensel, and K. Dilger, "Wire and arc additive manufacturing of aluminum components," *Metals (Basel).*, vol. 9, no. 5, pp. 1–9, 2019, doi: 10.3390/met9050608.

[11] G. Marinelli, F. Martina, S. Ganguly, and S. Williams, "Development of Wire + Arc additive manufacture for the production of large-scale unalloyed tungsten components," *Int. J. Refract. Met. Hard Mater.*, vol. 82, pp. 329–335, 2019, doi: 10.1016/j.ijrmhm.2019.05.009.

[12] R. Sun *et al.*, "Microstructure, residual stress and tensile properties control of wire-arc additive manufactured 2319 aluminum alloy with laser shock peening," *J. Alloys Compd.*, vol. 747, pp. 255–265, 2018, doi: 10.1016/j.jallcom.2018.02.353.

[13] F. Wang, S. Williams, P. Colegrove, and A. A. Antonysamy, "Microstructure and mechanical properties of wire and arc additive manufactured Ti-6Al-4V," *Metall. Mater. Trans. A Phys. Metall. Mater. Sci.*, vol. 44, no. 2, pp. 968–977, 2013, doi: 10.1007/s11661-012-1444-6.

[14] M. A. Jackson, A. Van Asten, J. D. Morrow, S. Min, and F. E. Pfefferkorn, "A Comparison of Energy Consumption in Wire-based and Powder-based Additive-subtractive Manufacturing," *Procedia Manuf.*, vol. 5, pp. 989–1005, 2016, doi: 10.1016/j.promfg.2016.08.087.

[15] M. K. Akbari, H. R. Baharvandi, and O. Mirzaee, "Nano-sized aluminum oxide reinforced commercial casting A356 alloy matrix: Evaluation of hardness, wear resistance and compressive strength focusing on particle distribution in aluminum matrix," *Compos. Part B Eng.*, vol. 52, pp. 262–268, 2013, doi: 10.1016/j.compositesb.2013.04.038.

[16] M. K. Surappa and P. K. Rohatgi, "Preparation and properties of cast aluminium-ceramic particle composites," *J. Mater. Sci.*, vol. 16, no. 4, pp. 983–993, 1981, doi: 10.1007/BF00542743.

[17] C. Gao, X. Chen, C. Su, and X. Chen, "Location dependence of microstructure and mechanical properties on wire arc additively manufactured nuclear grade steel," *Vacuum*, vol. 168, p. 108818, 2019, doi: 10.1016/j.vacuum.2019.108818.

[18] S. Fale, A. Likhite, and J. Bhatt, "Compressive, tensile and wear behavior of ex situ Al/AlN metal matrix nanocomposites," *J. Compos. Mater.*, vol. 49, no. 16, pp. 1917–1928, 2015, doi: 10.1177/0021998314540197.

[19] Wege R, Wortmann J (1989) Properties of single-crystal alloys for turbine blades. Mat-wiss u Werkstofftech 20:207–216

[20] Z. Qi, B. Qi, B. Cong, H. Sun, G. Zhao, and J. Ding, "Microstructure and mechanical properties of wire + arc additively

manufactured 2024 aluminum alloy components: As-deposited and post heat-treated," *J. Manuf. Process.*, vol. 40, no. February, pp. 27–36, 2019, doi: 10.1016/j.jmapro.2019.03.003.
[21] Ziebs J, Klingelhöffe H, Meersmann J, Frenz H (1998) Gesetzmäßigkeiten für die werkstoffmechanische Beschreibung der einkristallinen Nickelbasislegierung SC 16 unter ein- und mehrachsiger Beanspruchung, Berlin
[22] L. Wang, J. Xue, and Q. Wang, "Correlation between arc mode, microstructure, and mechanical properties during wire arc additive manufacturing of 316L stainless steel," *Mater. Sci. Eng. A*, vol. 751, no. February, pp. 183–190, 2019, doi: 10.1016/j.msea.2019.02.078.
[23] Y. Luo, J. Li, J. Xu, L. Zhu, J. Han, and C. Zhang, "Influence of pulsed arc on the metal droplet deposited by projected transfer mode in wire-arc additive manufacturing," *J. Mater. Process. Technol.*, vol. 259, pp. 353–360, 2018, doi: 10.1016/j.jmatprotec.2018.04.047.
[24] M. Liberini *et al.*, "Selection of Optimal Process Parameters for Wire Arc Additive Manufacturing," *Procedia CIRP*, vol. 62, pp. 470–474, 2017, doi: 10.1016/j.procir.2016.06.124.